Supporting Information

Ha et al. 10.1073/pnas.1214447109

SI Results

Detailed description of the mode of pseudosubstrate peptide binding. In all three structures the pseudosubstrate peptide binds in a similar fashion. Starting at the peptide N terminus, the conformation of R49 is extended into the acidic −2 peptide binding pocket and makes salt bridges to E507 and D444; this pocket is also bounded by S443 and T404. C-terminal to this, P50 fits tightly into a hydrophobic pocket bounded by W481, F516, T404, and Y480. The carbonyl oxygen of P50 points toward the ζ-amino group of K442. Next, K51 is extended away from the kinase domain. P52 takes the position of the phosphate acceptor residue and stacks against F461 and T478. L53 points away from the catalytic cleft and folds onto a hydrophobic patch formed by L475, M524, M482, and P479. Antiparallel β-stand hydrogen bonding is formed between L53 and G477 of the activation loop in a manner typical of kinase–peptide substrate interactions (1). The last residue visible in all three structures is V54, which stacks against a hydrophobic patch formed by L362, V476, F461, and aliphatic regions of the side chains for Q358 and R359. In two structures D55 is observed, and is extended away from the catalytic cleft. In total, the surface buries a total of between 1,054 and 1,211 $Å^2$ in the three structures (Protein Interfaces, Surfaces and Assemblies, PISA server) (2).

SI Discussion

Our kinase activity assays show that the region around P52 provides an autoinhibitory effect for the type II p21-activated kinases (PAKs). It is interesting, however, that in our assays we observe increased autoinhibition with longer constructs. For example, the 23-mer peptide provided a better inhibition than the short peptide RPKPLVDP (RPK) and $PAK4^{1–130}$ is the most potent N-terminal inhibitory construct; the reasons for this may be related to secondary or tertiary structures of these regions, or potential additional binding sites that are not visible in the electron density of our structures. Furthermore, the quadruple alanine mutation in PAK4-FL does not increase kinase activity to the level of the catalytic domain alone, although this difference may not be due to specific N-terminal interactions. We therefore conclude that the R^{49}PKP sequence is necessary and sufficient to inhibit kinase activity, but that there are potentially other regions of the kinase that can facilitate complete inhibition.

SI Materials and Methods

Expression and Purification. The PAK4 protein has four different alternative splicing proteins; we purchased cDNA for isoform 2 (Open Biosystems), which encodes a 426-aa protein (UniProt accession no. O96013-2). For our full-length PAK4 (PAK4-FL), we subcloned residues 5–426 into a modified pET-28 vector with an N-terminal hexahistidine (6xHis) tag removable by tobacco etch virus (TEV) protease. For our catalytic domain PAK4 (PAK4-cat), we subcloned residues 109–426 into the same expression vector. Because residues 121–426 of isoform 2 correspond exactly to residues 286–591 in isoform 1, for clarity we discuss kinase domain residues using the isoform 1 numbering throughout. We use isoform 2 numbering for residues in the N terminus (residues 1–119 are identical between isoform 1 and isoform 2). For purification of either recombinant PAK4-FL or PAK4-cat, we expressed N-terminal 6xHis-tagged proteins in BL21-CodonPlus(DE3)-RILP (containing extra copies of rare *Escherichia coli* argU, ileY, leuW, proL tRNA genes, which correct for codon bias and dramatically improve expression of sequences from other organisms) cells by induction with 0.5 mM IPTG (isopropyl β-D-1-thiogalactopyranoside) overnight at 18 °C. The harvested pellets were suspended in lysis buffer [20 mM Tris·HCl (pH 8.0), 100 mM NaCl, 1 mM Tris(2-carboxyethyl) phosphine (TCEP), and 0.1 mM PMSF] and lysed by sonication. The supernatants were affinity purified by HisTrap chelating column (GE Healthcare) and then resolved over Resource S (GE Healthcare) and Superdex 75 10/300GL (GE Healthcare) columns. Purified proteins were concentrated to 5 mg/mL in 20 mM Tris·HCl (pH 8.0), 150 mM NaCl, and 1 mM DTT with 1 mM phosphoaminophosphonic acid-adenylate ester (AMP-PNP) and 5 mM $MgCl_2$ for crystallization trials.

For kinase assays, we subcloned specific regions of PAK4 into a modified pMCSG9 vector that includes an N-terminal 6xHis tag followed by maltose binding protein (MalBP) and a TEV protease cleavage site. Using this vector we generated PAK4 constructs PAK4-$cat^{135–426}$, $PAK4^{1–30}$, $PAK4^{1–45}$, $PAK4^{1–70}$, $PAK4^{1–90}$, $PAK4^{1–130}$, $PAK4^{31–130}$, $PAK4^{80–130}$, and $PAK4^{110–130}$. We used the QuikChange (Agilent Technologies) site-directed mutagenesis kit to introduce point mutations that allowed generation of PAK4 constructs PAK4-FL^{4A}, $PAK4^{1–70\text{-}4A}$, and $PAK4^{1–130\text{-}4A}$. For expression, the 6xHis-MalBP-tagged PAK4 N-terminal constructs and the 6xHis-tagged PAK4-FL^{4A} were induced with 0.5 mM IPTG overnight at 18 °C. Following resuspension in lysis buffer and lysis by sonication, the truncated proteins were purified by HisTrap chelating column (GE Healthcare) and dialyzed against 20 mM Tris·HCl (pH 8.0), 150 mM NaCl, and 1 mM DTT. Short peptides RPK and QKFTGLPRQW (QKF) and 23-mer peptides SARRPKPLVDPACITSIQPGAPK and SARAAAALVDPACAASIQPGAPK were synthesized and HPLC purified at Tufts University Core Facility.

We purchased cDNA for PAK6 (UniProt accession no. Q9NQU5; Open Biosystems) and subcloned the catalytic domain, residues 383–674, into a modified pET-32 vector with an N-terminal 6xHis tag cleavable by TEV protease. Recombinant PAK6-cat was expressed in BL21-CodonPlus(DE3)-RILP cells following induction with 0.5 mM IPTG overnight at 18 °C. The harvested pellet was resuspended in lysis buffer [20 mM Tris·HCl (pH 8.0), 100 mM NaCl, 1 mM TCEP, and 0.1 mM PMSF] and lysed by sonication. The supernatant was affinity purified by HisTrap chelating column (GE Healthcare) and dialyzed against a buffer of 20 mM Tris·HCl (pH 8.0), 150 mM NaCl, and 1 mM DTT.

PAK4 Crystallization and Data Collection. ***P3 crystal form.*** PAK4-cat crystals crystallize in 0.1 M Mes (pH 6.0), 0.6–0.7 M K/Na tartrate at room temperature. For cocrystallization of the *P*3 crystal form PAK4-cat crystals with RPK peptide, we preincubated PAK4-cat with RPK peptide in a 1:1.5 ratio. The RPK peptide cocrystals were subjected to dehydration by 18-h vapor equilibration against Mes (pH 6.0), 1 M K/Na tartrate. Cryoprotectant buffer contained reservoir buffer plus 25–30% (vol/vol) glycerol. Data were collected at the Advanced Photon Source (APS) beamline 24-ID-C and at the National Synchrotron Light Source (NSLS) beamline X29.

$P4_12_12$ crystal form. PAK4-cat crystals were grown using hanging-drop vapor diffusion methodology by mixing a 1:1 volume ratio of purified PAK4-cat and reservoir solution containing Tris·HCl (pH 7.5), 1.5–2.0 M Na acetate at room temperature. For cocrystallization of PAK4-cat with RPK and QKF peptides, we preincubated PAK4-cat with either RPK peptide or QKF peptide in ratios of 1:1.5. We obtained optimized conditions for PAK4-cat with RPK peptide or QKF peptide at conditions of 0.1 M Tris·HCl (pH 7.5) and 1.5–2.0 M Na acetate. Before flash-freezing, the crystals were equilibrated over 2.5 M Na acetate as a cryoprotectant. Data were collected at APS beamline 24-ID-C and NSLS beamline X6A.

Structure Determination and Refinement. Crystallographic data were processed using the HKL2000 package (3). We generated initial phases by molecular replacement using the program Phaser (4) using the previously determined crystal structure of PAK4 catalytic domain (PDB ID code 2CDZ) (5) as the search model. Refinements were conducted using Refmac5 (6) with a maximum-likelihood target, two TLS (translation, libration, screw) groups per molecule, and medium noncrystallographic symmetry restraints. Model-building was conducted in Coot (7) and model validation using MolProbity (8) with all built residues within favored or allowed Ramachandran regions. Good electron density is observed for each of the kinase domains, although bound AMP-PNP could only be built for the *P*3 structures (Table S1).

In Vitro PAK4 Kinase Assay. The activity of recombinant PAK4-cat$^{135–426}$, purified as described above, was considered optimally active, and the effects of purified recombinant PAK4 N-terminal constructs or synthesized peptides were tested. Kinase assays were performed by adding 150 nM of kinase (purified PAK4-cat$^{135–426}$, crystallization-quality PAK4-FL, or PAK6-cat), 2 μM of myelin basic protein (MBP) as the substrate, 50 μM of cold ATP and 0.1 μCi of hot [γ-^{33}P]ATP in Tris buffer [20 mM Tris·HCl (pH 8.0), 0.15 M NaCl, 1 mM DTT, and 10 mM $MgCl_2$], total volume 25 μL. Transinhibition assays included 15 μM of purified PAK4 N-terminal constructs; 15 μM of purified MalBP control; 150 μM of purified RPK or QKF peptides; or 75 μM of purified 23-mer or 23-mer^{6A} peptides. The reaction was conducted at 30 °C for 10 min and stopped by addition of 5× sample buffer and analyzed by SDS/PAGE. Gels were analyzed by exposure to phosphor storage screen (GE Healthcare) followed by scanning using a Molecular Imager FX Pro Plus System (Bio-Rad) and quantification by optical densitometry Quantity One (Bio-Rad). Measured activities were controlled for addition of MalBP. Relative activities were compared with those measured for PAK4-cat$^{135–426}$. Measurements were calculated from at least three independent experiments. Significant differences were calculated by *t* test (two-sample, assuming equal variances).

CDC42 (residues 1–177) and RAC1 (residues 1–177) were expressed as N-terminal 6xHis-tagged proteins, purified by Ni-affinity, and dialyzed against 20 mM Tris·HCl (pH 8.0), 0.15 M NaCl, 1 mM DTT; they were added at concentrations of 15 μM with GMP-PNP (5′-guanylyl imidodiphosphate) 1 mM and Mg^{2+} 10 mM.

β-PIX SH3 domain (residues 184–243) was subcloned from its cDNA (UniProt accession no. Q14155; Open Biosystems) into a modified pET-28 vector with an N-terminal 6xHis tag removable by TEV protease, and Src SH3 domain (residues 85–143) was subcloned into a modified pET-28 vector with an N-terminal 6xHis tag removable by TEV protease. Both β-PIX SH3 and Src SH3 were expressed in BL21-CodonPlus(DE3)-RILP cells by induction with 0.5 mM IPGT overnight at 18 °C. The harvested pellets were suspended in lysis buffer [20 mM Tris·HCl (pH 8.0), 100 mM NaCl, 1 mM TCEP, and 0.1 mM PMSF] and lysed by sonication. The supernatants were affinity purified by HisTrap chelating column (GE Healthcare) and then dialyzed against a buffer of 20 mM Tris·HCl (pH 8.0), 150 mM NaCl, and 1 mM DTT for kinase activity assays; they were added at concentrations of 15 μM in the kinase assay with PAK4-FL at a concentration of 150 nM.

BAD Assay. HEK 293 cells in 12-well plates were cotransfected with 1 μg pEBG-BAD (which produces murine BAD as a GST fusion protein) and 0.6 μg of empty pEGFP, pEGFP-PAK4, pEGFP-PAK4^{4A}, or pEGFP-PAK4-cat using Lipofectamine 2000 (Invitrogen) as recommended by the manufacturer. After 24 h, cells were serum starved (0.1% FBS) for 3 h, treated with wortmannin (250 nM) for 30 min, and lysed in buffer containing 20 mM Tris (pH 7.5), 150 mM NaCl, 1 mM EDTA, 1 mM EGTA, 1% (vol/vol) Triton ×100, 2.5 mM sodium pyrophosphate, 1 mM β-glycerophosphate, 1 mM Na_3VO_4, 1 mM DTT, 1 mM PMSF, 10 μg/mL leupeptin, 2 μg/mL pepstatin A, and 10 μg/mL aprotinin. Clarified lysates were then rotated with Glutathione Sepharose 4B (GE Healthcare) for 1 h at 4 °C. Resin was washed twice with ice-cold lysis buffer, suspended in Laemmli sample buffer, and heated to 95 °C for 10 min. Precipitated protein and cell lysates were subjected to SDS/PAGE and transferred to PVDF membrane. Pull-down samples were probed with mouse anti-GST (Cell Signaling Technology) and rabbit anti-BAD pS112 (Cell Signaling Technology) antibodies. Lysates were probed with mouse anti-GFP (Clontech) followed by enhanced chemiluminescence.

Cell Morphology. NIH 3T3 cells in six-well plates were transfected with pEGFP, pEGFP-PAK4, or pEGFP-PAK4^{4A} (1 μg per well) using Lipofectamine PLUS (Invitrogen) as recommended by the manufacturer. Cells were examined by fluorescence microscopy at 40× magnification and photographed 24 h following transfection.

Confocal Imaging. COS-7 cells were transiently transfected at 90% confluence in 10-cm plates with 1 μg pEGFP-PAK4^{WT} and PAK4^{4A} constructs using FuGENE HD (Roche) transfection reagent according to the manufacturer's instructions. Following transfection, cells were detached and plated in 24-well trays on Fisherbrand No. 1.5 Coverslips (catalog no. 12-545-81; Thermo Fisher) and cultured in DMEM supplemented with 10% (vol/vol) FBS and 1% (vol/vol) penicillin/streptomycin for 24 h to recover from transfection. Cells on coverslips were washed 3× with Dulbecco's PBS (DPBS), then fixed by incubating cells for 15 min at room temperature in 0.5 mL freshly prepared paraformaldehyde (3.2%). Cells were then washed 3× with DPBS and incubated at room temperature for 1 h in permeabilization buffer (0.5% Triton X-100 in a 1% BSA). After incubation, cells were stained in permeabilization buffer containing 2.5 U/mL tetramethylrhodamine (TRITC)-conjugated phalloidin (catalog no. R415; Invitrogen) for 20 min, then washed 3× with DPBS. Cells were examined with a multicolor spinning-disk confocal UltraVIEW VoX system (Perkin-Elmer). Images were analyzed and processed using Velocity software.

Pull-Down Assay. N-terminal His-tagged RAC1 and CDC42 were preincubated with 1 mM GTP and 5 mM $MgCl_2$ for 10 min at 4 °C in a PBS buffer. A total of 5 μg of purified PAK4$^{1–70}$ (N-terminally tagged with 6xHis and MalBP) was loaded to amylose beads. After washing beads with PBS buffer 3×, 5 μg of GTP-loaded RAC1 or CDC42 were loaded to the beads pellet. Following 30 min incubation at 4 °C in a PBS buffer, the pellets were washed 3× and the bound proteins were eluted with SDS sample buffer at 95 °C and analyzed by Western blot with anti-polyHistidine antibody (clone HIS-1, H1029; Sigma-Aldrich). A total of 1 μg of His-MBP-PAK4$^{1–70}$, His-CDC42, and His-RAC1 were included as controls (Fig. S5).

1. Yang J, et al. (2002) Molecular mechanism for the regulation of protein kinase B/Akt by hydrophobic motif phosphorylation. *Mol Cell* 9:1227–1240.
2. Krissinel E, Henrick K (2007) Inference of macromolecular assemblies from crystalline state. *J Mol Biol* 372:774–797.
3. Otwinowski Z, Minor W (1997) Processing of X-ray diffraction data collected in oscillation mode. *Meth Enzymol* 276(Pt A):307–326.
4. McCoy AJ, Grosse-Kunstleve RW, Storoni LC, Read RJ (2005) Likelihood-enhanced fast translation functions. *Acta Crystallogr D Biol Crystallogr* 61:458–464.
5. Eswaran J, et al. (2007) Crystal structures of the p21-activated kinases PAK4, PAK5, and PAK6 reveal catalytic domain plasticity of active group II PAKs. *Structure* 15:201–213.
6. Murshudov GN, Vagin AA, Dodson EJ (1997) Refinement of macromolecular structures by the maximum-likelihood method. *Acta Crystallogr D Biol Crystallogr* 53:240–255.
7. Emsley P, Cowtan K (2004) Coot: Model-building tools for molecular graphics. *Acta Crystallogr D Biol Crystallogr* 60:2126–2132.
8. Davis IW, Murray LW, Richardson JS, Richardson DC (2004) MOLPROBITY: Structure validation and all-atom contact analysis for nucleic acids and their complexes. *Nucleic Acids Res* 32(Web Server issue):W615–W619.

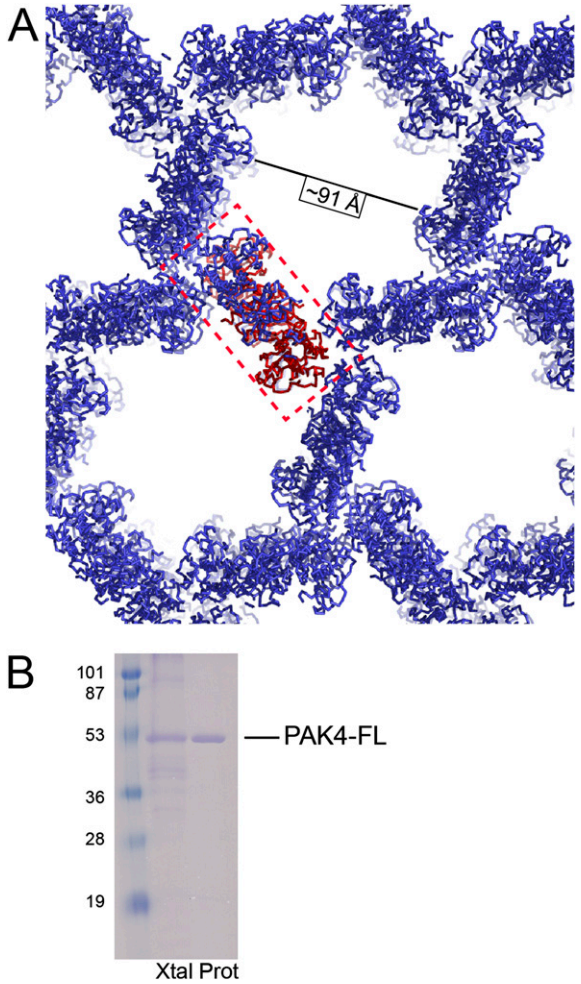

Fig. S1. PAK4-FL crystals. (*A*) Crystal packing for PAK4-FL crystals in space group *P*3. The solvent channels are ~91 Å in diameter and constitute ~80% of the crystal. PAK4-cat also crystallizes in this crystal form. Red box indicates asymmetric unit, with both molecules in the asymmetric unit colored red. (*B*) SDS/PAGE of PAK4-FL crystals. A PAK4-FL crystal was looped and washed 6× in 2-μL drops of distilled water, then run on 15% SDS/PAGE. Lane "Xtal" indicates the PAK4-FL crystal; lane "Prot" indicates purified PAK4-FL protein.

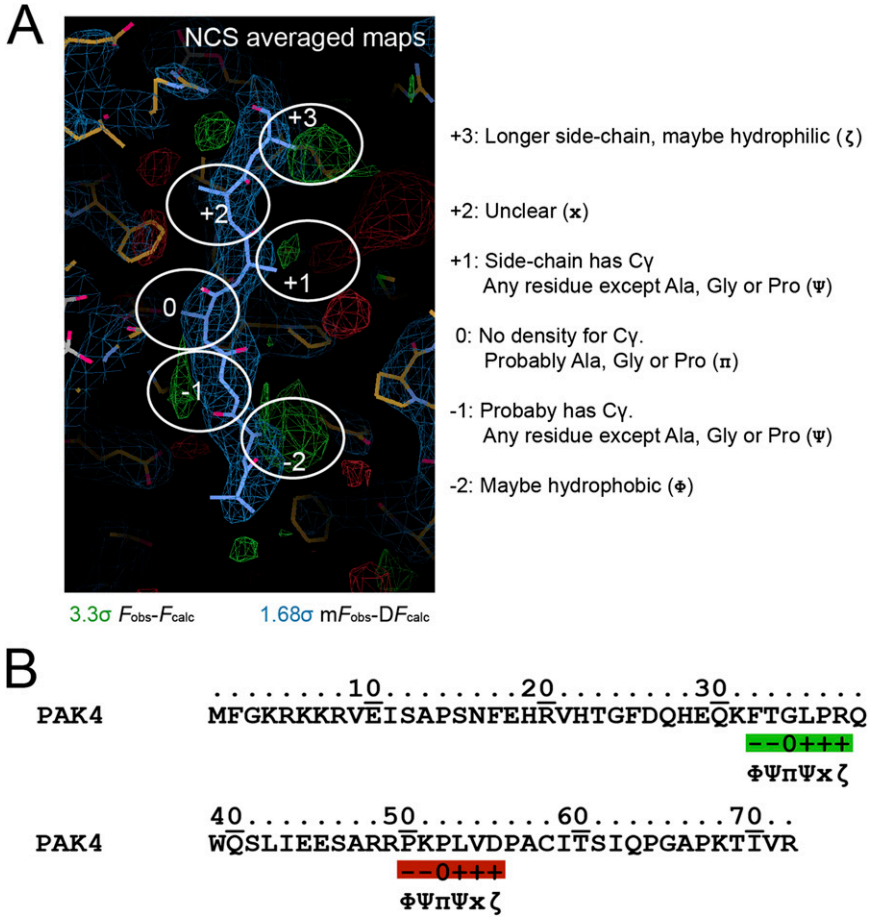

Fig. S2. Hypothesis generation for bound peptide in PAK4-FL crystals. (*A*) Noncrystallographic symmetry (NCS)-averaged electron density maps for PAK4-FL crystals. A polyalanine chain was built into the positive difference density (shown in Fig. 2*B*) for both copies in the asymmetric unit. The maps were then NCS averaged, and regions of high difference density used for hypothesis generation for the bound peptide sequence. Positions are labeled −2 to +3, with position 0 at the location of the phosphoacceptor site. Contoured at 3.3σ for the F_{obs}-F_{calc} and 1.68σ for the mF_{obs}-DF_{calc} NCS-averaged maps. Image generated in Coot. (*B*) The hypothetical sequence was then cross-referenced with the N terminus of PAK4, and two potential matches were discovered. QKF peptide match shown in green; RPK peptide match shown in red.

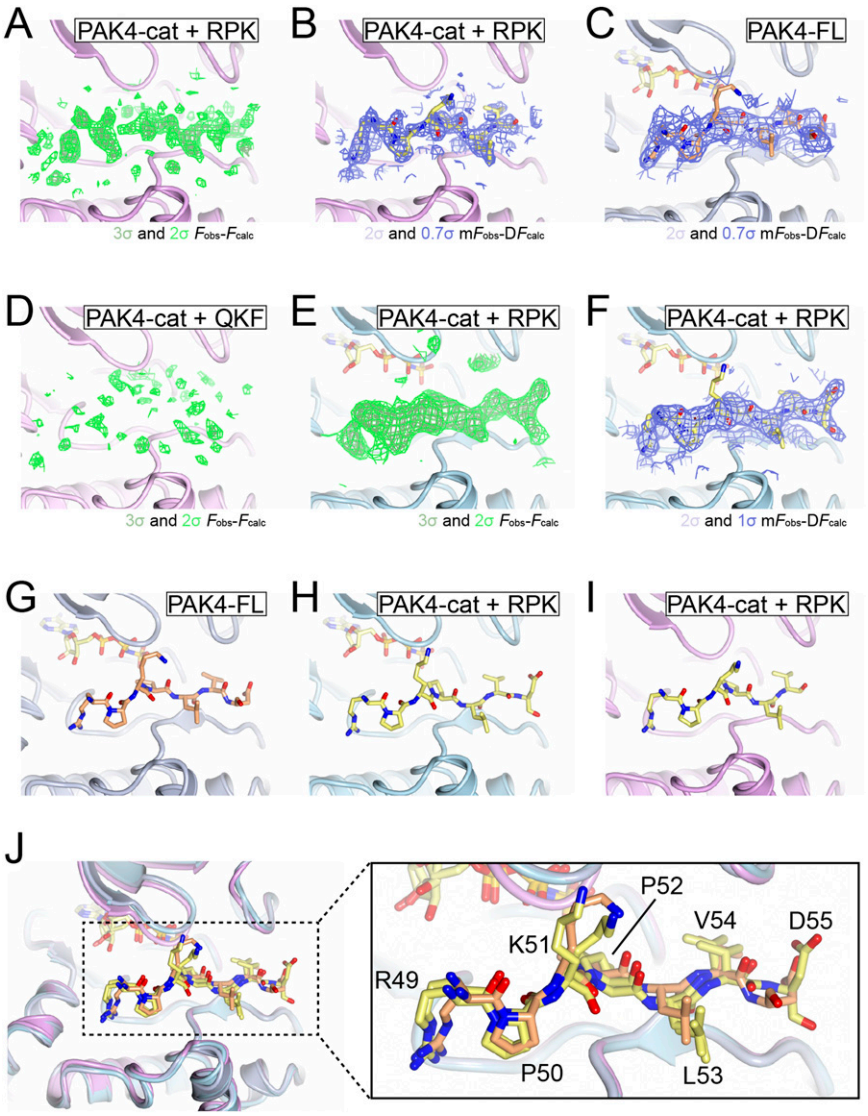

Fig. S3. Structures of PAK4. (*A* and *B*) PAK4-cat with RPK peptide. $P4_12_12$ crystal form of PAK4 cocrystallized with the RPK peptide. (*A*) Two contour levels (2σ and 3σ in dark and light green, respectively) for the unbiased F_{obs}-F_{calc} map. Bound peptide is clearly observed in the PAK4-cat + RPK structure. (*B*) Final refined mF_{obs}-DF_{calc} density (0.7σ and 2σ in dark and light blue, respectively). (*C*) Final refined density for PAK4-FL *P*3 crystal. mF_{obs}-DF_{calc} density (0.7σ and 2σ in dark and light blue, respectively) is shown. (*D*) PAK4-cat with QKF peptide. $P4_12_12$ crystal form of PAK4 cocrystallized with the QKF peptide. Two contour levels (2σ and 3σ in dark and light green, respectively) are shown for the unbiased F_{obs}-F_{calc} map following refinement to convergence for the rest of the structure, but with no atoms built, or refined, in this region. Peptide is not observed in the PAK4-cat + QKF structure. (*E* and *F*) PAK4-cat with RPK peptide. *P*3 crystal form of PAK4 cocrystallized with RPK peptide. Clear difference density is observed in the peptide substrate binding site. (*E*) Unbiased F_{obs}-F_{calc} density (2σ and 3σ in dark and light green, respectively). (*F*) Final refined mF_{obs}-DF_{calc} density (1σ and 2σ in dark and light blue, respectively). (*G*–*I*) Cartoon diagrams showing binding of autoinhibitory peptide to PAK4 kinase domain. Bound AMP-PNP and N-terminal peptide are shown in stick format. (*G*) Final refined PAK4-FL *P*3 crystal form. (*H*) PAK4-cat cocrystallized with RPK peptide, *P*3 crystal form. (*I*) PAK4-cat cocrystallized with RPK peptide, $P4_12_12$ crystal form. (*J*) Superposition of the refined structures shown in *G*–*I*. The final refined structures very closely superpose.

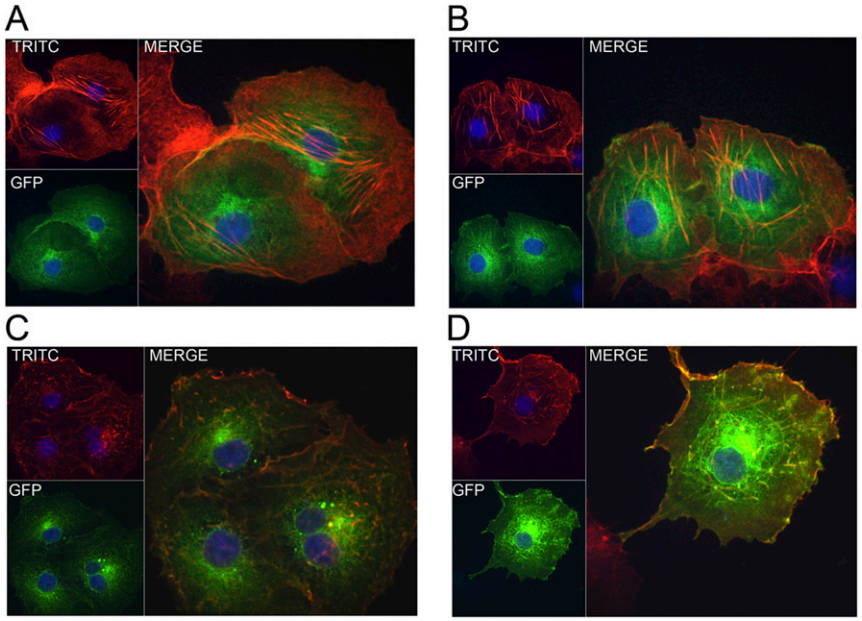

Fig. S4. Actin containing stress fiber organization in ectopic pEGFP-PAK-FL and pEGFP-PAK4-FL^{4A} expressing COS-7 cells. (*A* and *B*) COS-7 cells were transiently transfected with pEGFP-PAK-FL or (*C* and *D*) pEGFP-PAK4-FL^{4A}. (*A–D*, *Upper Left*) Actin-containing stress fibers were investigated through staining with TRITC-conjugated phalloidin (labeled TRITC). (*A–D*, *Lower Left*) Localization of pEGFP-PAK4 protein (labeled GFP). (*A–D*, *Right*) Spatial overlap (labeled Merge). In TRITC and Merge panels, a marked reduction of actin-containing stress fibers was seen in pEGFP-PAK4-FL^{4A}–expressing cells (*C* and *D*), whereas pEGFP-PAK-FL (*A–D*) TRITC and Merge panels showed robust actin-containing stress fibers.

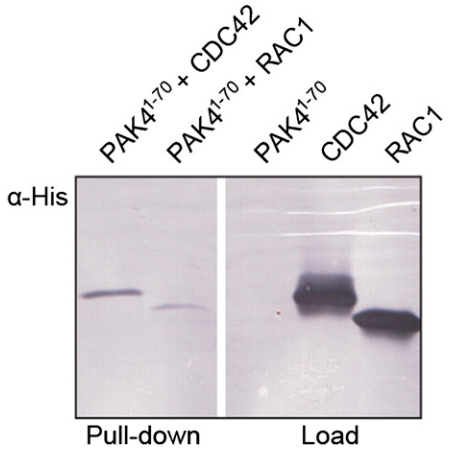

Fig. S5. Pull-down assay between PAK4$^{1–70}$ and GTPases. A total of 5 μg of purified PAK4$^{1–70}$ (N-terminally tagged with 6xHis and MalBP) was loaded to amylose beads and incubated with GTP-loaded RAC1 or CDC42. Bound proteins were eluted with SDS sample buffer at 95 °C and analyzed by Western blot with anti-polyHistidine antibody. A total of 1 μg of His-MBP-PAK4$^{1–70}$, His-CDC42, and His-RAC1 were included as controls. White line indicates break in continuous gel.

Table S1. Detailed data collection and refinement statistics

	PAK4-FL (PDB ID code 4FIE)	PAK4-cat + RPK peptide (PDB ID code 4FIF)	PAK4-cat (PDB ID code 4FIG)	PAK4-cat + QKF peptide (PDB ID code 4FIH)	PAK4-cat + RPK peptide (PDB ID code 4FII)	PAK4-cat (PDB ID code 4FIJ)
Data collection						
Space group	*P*3	*P*3	*P*3	$P4_12_12$	$P4_12_12$	$P4_12_12$
X-ray source	APS 24-ID-C	NSLS X29	APS 24-ID-C	NSLS X6A	NSLS X6A	APS 24-ID-C
Detector	ADSC Q315	ADSC Q315	ADSC Q315	ADSC Q270	ADSC Q270	ADSC Q315
Wavelength, Å	0.97918	1.0750	0.97918	0.97550	0.97550	0.97918
Unit cell						
a, b, c, Å	141.5, 141.5, 61.9	141.4, 141.4, 61.6	141.9, 141.9, 61.9	61.7, 61.7, 181.5	61.6, 61.6, 181.8	61.4, 61.4, 177.3
α, β, γ, °	90, 90, 120	90, 90, 120	90, 90, 120	90, 90, 90	90, 90, 90	90, 90, 90
Resolution range (Å)*	50.0–3.1 (3.2–3.1)	50.0–2.6 (2.69–2.6)	50.0–3.0 (3.1–3.0)	50.0–1.97 (2.04–1.97)	20.0–2.0 (2.07–2.0)	50.0–2.3 (2.38–2.3)
No. of unique reflections	25,023	42,196	27,710	25,818	24,673	15,998
Completeness (%)*	96.1 (83.6)	99.6 (98.9)	100 (100)	99.5 (96.1)	100 (100)	98.7 (95.0)
R_{sym} (%)*	15.4 (0.0)	8.8 (88.7)	31.7 (0.0)	7.2 (59.3)	11.4 (77.8)	8.1 (34.7)
Mean σ*	11.1 (1.2)	17.5 (1.8)	6.5 (1.3)	36.8 (3.9)	25.4 (3.6)	24.5 (2.3)
Wilson *B*-factor	101.4	65.1	84.9	29.0	31.0	39.6
Redundancy	6.6 (3.9)	4.8 (4.1)	4.8 (3.9)	11.4 (10.3)	14.1 (14.0)	8.6 (4.3)
Refinement statistics						
Resolution range* (Å)	46.6–3.1 (3.18–3.1)	46.5–2.6 (2.67–2.60)	50.0–3.0 (3.09–3.0)	50–1.97 (2.02–1.97)	20.0–2.0 (2.05–2. 0)	50.0–2.3 (2.36–2.3)
R_{factor} (%)*	25.6 (36.3)	20.6 (33.0)	19.6 (30.9)	17.8 (22.2)	20.1 (29.3)	20.7 (43.3)
Free R_{factor} (%)*	27.6 (38.7)	22.7 (35.9)	22.1 (34.0)	22.5 (27.7)	24.0 (40.0)	27.1 (49.1)
Free *R* reflections (%)*	5.0 (5.4)	5.1 (5.9)	5.0 (5.9)	5.1 (5.6)	5.1 (5.1)	5.0 (5.0)
Free *R* reflections, no.*	1,197 (76)	2,126 (173)	1,396 (115)	1,301 (84)	1,246 (76)	776 (46)
Residues built						
Expressed PAK4	A/49–55, 297–590 B/49–55, 297–590	A/296–589 B/297–589	A/298–590 B/298–590	A/298–589	A/299–590	A/299–590
Cocrystallized peptide		C/49–55 D/49–55		Not visible in the electron density	B/49–54	
No. water molecules	2	59	19	239	161	40
Mean *B*-factor, Å^2						
Protein (A/B)	93.1/93.1	70.8/70.5	88.1/88.0	30.0	30.8	60.2
AMP-PNP (A/B)	110.1/106.8	66.2/65.6	85.9/83.3	—	—	—
Mg^{2+} (A/B)	—	—	98.9/95.7	—	—	—
Peptide (C/D)	—	84.8/81.9	—	—	59.4	—
H_20	66.4	55.6	70.9	37.4	33.9	56.4
Model statistics						
Rmsd bond lengths, Å	0.005	0.005	0.005	0.019	0.018	0.007
Rmsd bond angles, °	0.992	0.958	1.042	2.014	2.022	1.248
Ramachandran plot: favored/allowed/ disallowed, %	95.2/4.4/0.3	97.6/2.4/0	97.4/2.6/0	99.3/0.7/0	98.3/1.7/0	96.9/3.1/0

*High-resolution shell.